Reconfigurable Reflectarray Using Addressable Metamaterials

Thomas H. Hand, *Student Member, IEEE*, and Steven A. Cummer, *Senior Member, IEEE*

***Abstract*—We develop a reconfigurable reflectarray using digitally addressable complementary electric *LC* (CELC) metamaterials. The surface is composed of addressable CELC resonators, which are tuned to achieve a spatial gradient in the reflection coefficient phase angle. This gradient is used to deflect normally incident plane waves in a controlled nonspecular direction.**

***Index Terms*—Frequency selective surfaces, metamaterials, reflectarrays.**

I. Introduction

ENGINEERED structures called metamaterials can be designed to exhibit interesting electric and magnetic responses typically not observed in conventional materials. They are typically realized using subwavelength particles with an electromagnetic resonance [1], [2]. The ability for media to possess positive and negative values of electric permittivity and magnetic permeability is useful in a variety of applications, such as electronic phase shifting and compensation [3], [4] and forming a perfect lens [5]. The standard metamaterial particle to achieve a negative magnetic response is the split-ring resonator (SRR), which is a capacitively loaded loop that is an effective *LC* tank circuit when much smaller than the operating wavelength [2]. The electric counterpart of the SRR is the electric *LC* resonator (ELC), which was proposed to achieve a resonant electric permittivity [6].

Reflectarrays have a wide variety of applications in radar systems and antennas [7], [8] such as radomes [9], reflectors, electromagnetic interference (EMI) shielding, and radar absorbent materials (RAM) [10], [11]. Typically composed of periodic two-dimensional arrays of elements with spacing on the order of $\lambda_0/2$, conventional designs employ circular, rectangular dipole, cross-dipole, tripole, ring, square, and gridded square loop unit cell geometries [12]. References [13] and [14] develop analytical methods for understanding the transmission and reflection properties of metamaterial reflectarrays (metasurfaces) in terms of the unit cell electric and magnetic polarizabilities.

In this letter, we develop a reconfigurable reflectarray using the complementary ELC resonator (CELC) metamaterial. In controlled scattering and beam-steering applications, important figures of merit for reflectarrays are the phase and magnitude swings in the surface reflection coefficient for each element in the array. The phase swing $\Delta\Gamma_{\mathrm{p}}$ is the range of achievable reflection coefficient phase angles, and the magnitude swing $\Delta\Gamma_{\mathrm{m}}$ is the range of achievable reflection coefficient magnitudes. To steer incident plane waves over a large range of directions, it is desirable for each element in the reflectarray to have a large $\Delta\Gamma_{\mathrm{p}}$. An approach to a reconfigurable reflectarray can be found in [15], which demonstrates a $\pm 30^\circ$ beam deflection with $\Delta\Gamma_{\mathrm{p}} = 325^\circ$ and $\Delta\Gamma_{\mathrm{m}} = 3.5$ dB at $f = 5.8$ GHz using a cell spacing of $0.55\lambda_0$. Recent work on conventional reflectarrays in [16] reported a phase swing $\Gamma_{\mathrm{p}} = 180^\circ$ to deflect a plane wave $\theta' = 20^\circ$ using a $0.6\lambda_0$ element spacing. Metamaterial approaches to frequency selective surfaces and reflectarrays include the work found in [17], which reported maximum beam deflection of $\theta' = 30^\circ$ using a tunable electromagnetic band-gap (EBG) metamaterial approach with an element spacing of $\lambda_0/7$. Other papers have explored using different metamaterial configurations [18], [19]. Reconfigurable reflectarrays using microstrip patches loaded with RF microelectromechanical systems (MEMS) switches have been developed in [20], where it was shown that $\Delta\Gamma_{\mathrm{p}} = 150^\circ$ (tuned in discrete increments) and $\Delta\Gamma_{\mathrm{m}} < 1.5$ dB at $f = 2$ GHz.

The CELC particle is a suitable element to be used in the reflectarray because its reflection characteristics are invariant over a wide range of incident angles [21], and it can realize a large reflection coefficient phase swing ($\Delta\Gamma_{\mathrm{p}} \approx 340^\circ$). Adhering to the standard definition of a metamaterial, the CELC is electrically small with largest dimension $\ll \lambda_0$. This means that the reflectarray can contain a higher density of resonators, which can yield a steeper phase gradient for a given surface size. Because the single-element spacing is electrically small, the metamaterial reflectarray can more closely approximate a continuous phase profile than the conventional reflectarray.

II. Behavior of the CELC Particle

The fundamental resonance of the CELC particle is driven by an in-plane magnetic field, the dual behavior of the ELC [21]. The resonance of the CELC leads to a transmission magnitude passband, the dual response of its complementary particle, the ELC [6]. Because of the transmission magnitude passband, a stopband in the reflection coefficient magnitude is observed. Near the CELC resonance, the reflection phase changes over a broad range of angles, and it is this property of the CELC that we are interested in tuning to control the scattering of incident electromagnetic energy. We compare the CELC metasurface to a perfect electric conducting (PEC) sheet, which has a unity reflection coefficient magnitude $\Gamma_{\mathrm{m}} = 1$ and constant phase $\Gamma_{\mathrm{p}} = 180^\circ$. The difference between the metal plate and the addressable CELC surface is that the spatial reflection coefficient phase angle of the CELC surface can be controlled, which

Manuscript received October 08, 2009; manuscript revised November 22, 2009 and January 14, 2010. Date of publication February 17, 2010; date of current version March 05, 2010.

The authors are with the Department of Electrical Engineering and the Center for Metamaterials and Integrated Plasmonics, Duke University, Durham, NC 27708 USA (e-mail: thh5@duke.edu; cummer@ee.duke.edu).

Digital Object Identifier 10.1109/LAWP.2010.2043211

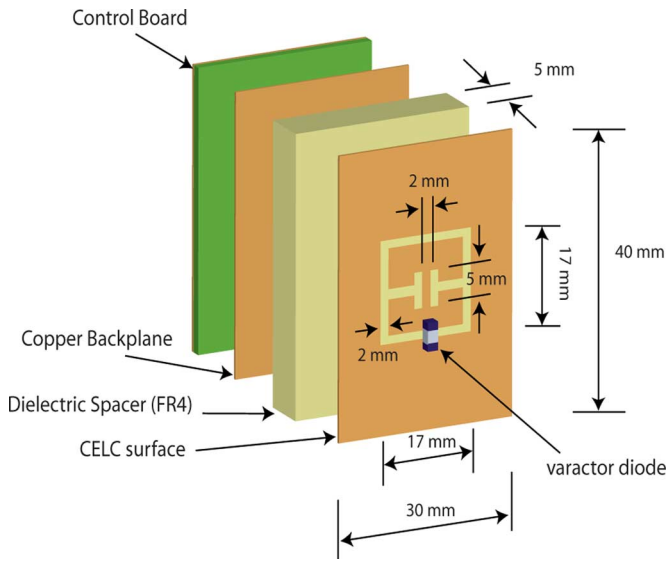

Fig. 1. Schematic of a single element used in the addressable CELC reflectarray. The CELC particle on the top layer is loaded with a varactor diode to tune its self resonant frequency. The FR4 dielectric spacer is used to tune the resonance as well as absorb transmitted energy. The control board contains the addressable circuitry used to control each varactor diode. The bias is applied to each diode using vias from the control board to the CELC reflectarray.

causes incident plane waves to scatter in a nonspecular direction. This behavior can be exploited in a wide variety of applications requiring controlled scattering and dispersing of microwave radiation, such as (RCS) control and reduction [22].

The resonant frequency of the CELC particle can be tuned using a microwave varactor diode. As shown in Fig. 1, the microwave varactor diode is placed between the two isolated copper conductors of the CELC so that a reverse dc bias can be applied. As the reverse bias across the varactor diode is increased, its capacitance decreases [23]. The varactor tunes the effective capacitance of the CELC particle, which in turn tunes its self-resonant frequency. The bias across each cell can be individually controlled using a one-wire addressable line [24], which allows the local reflection coefficient phase at any element across the surface to be independently tuned. This is useful since tight control over the local reflection coefficient phase controls the fields scattered from the surface.

III. Analysis of the CELC Metasurface Reflectarray

The surface of CELC elements is treated as a phased-array antenna, with the incident electromagnetic wave as the source and the array factor (in the θ-plane for the feed placed normal to the plane of the array)

$$F(\theta) = \sum_{n=1}^{N} \exp(j(nk_0 d \sin\theta + \psi_n)) \tag{1}$$

determining the angular distribution of radiated electromagnetic energy. In (1), N is the total number of elements in the array, k_0 is the free-space wave vector, d is the element spacing, ψ_n is the phase shift associated with each element, and θ is the azimuthal angle. In (1), it is assumed that all elements have a unity amplitude weight. The radiated electric field is related to $F(\theta)$ by $E_{\rm rad}(\theta) = E_{\rm element}(\theta)F(\theta)$, and the radiated power is proportional to $|F(\theta)|^2$. The angular distribution of the scattered fields will consist of one main beam with sidelobes. Selection of the ψ_n is critical in determining the distribution of $E_{\rm rad}(\theta)$, and this phase profile must obey a certain relationship to shift the field maximum away from the specular direction. Finding the critical points of $|F(\theta)|^2$ in (1) will help us locate the directions θ' of maximum radiation. Setting $\partial|F(\theta)|^2/\partial\theta = 0$ and setting $\theta = \theta'$ (some arbitrary direction we wish to steer the field maximum to) leads to the phase profile constraint

$$\psi_n = \frac{\pi}{4} - nk_0 d \sin\theta'. \tag{2}$$

Thus, for a given element spacing d and desired beam tilt angle $\theta = \theta'$, (2) predicts the required phase distribution across the surface to steer the peak scattered field to θ'. Given that we know from (2) what reflection phase angles are needed to steer the maximum radiated power in some direction θ', it is necessary to know what phase values are accessible with the varactor-loaded CELC. Ansoft HFSS simulations were used to determine the CELC element geometry to excite a resonance between 2–3 GHz. This frequency range was chosen because of the convenience of free-space measurements. The Skyworks SMV 1405-079 hyperabrupt junction varactor diode was loaded on each CELC of the reflectarray. The capacitance of the hyperabrupt junction diode follows the form $C(V) = \alpha_0/(\beta + V)^n$, where V is the applied reverse bias, $\alpha_0 = C_0\delta^{-n}, \beta = 1/\delta, C_0$ is the zero-bias capacitance, δ is the built-in potential across the diode, and n is the tuning slope [23]. The parameters α_0, β, and n were determined by fitting $C(V)$ to the data provided from the SMV 1405-079 data sheet, where it was found that $\alpha_0 = 2.27, \beta = 0.65$, and $n = 0.375$ provided a close fit with the measured values from the varactor data sheet. The SMV 1405–079 capacitance tunes down from 2.67 to 0.63 pF when biased from 0–30 V. This *CV* relation was used to estimate the varactor bias needed to achieve the necessary capacitance for the required phase angle ψ_n. The simulated reflection coefficient magnitude and phase for the CELC design of Fig. 1 is shown in Fig. 3. The plots are shown between 2.2–2.3 GHz for varactor capacitances between 0.936 and 1.038 pF. At $f = 2.25$ GHz, the reflection phase swing $\Delta\Gamma_{\rm p}$ is over 200°, but when the full range of capacitances (0.63–2.67 pF, not shown) are used, $\Delta\Gamma_{\rm p}$ is about 340°. It is also important to note the large reflection magnitude variation $\Delta\Gamma_{\rm m}$ at $f = 2.25$ GHz is about 20 dB. While this is quite large and unavoidable due to the resonant nature of the CELC, it does not significantly affect the peak of the relative scattered power distribution. Such a large $\Delta\Gamma_{\rm m}$ leads to larger sidelobe levels and a broader beamwidth, which can be verified by inputting the magnitude distribution into (1).

IV. Fabrication and Measurements

For the experiment, a surface consisting of 25 CELCs (5×5 elements) was fabricated. Vias were drilled from the control layer behind the copper backplane to the CELC surface to bias each varactor. The surface (shown in Fig. 2) has a control bus containing lines for +30 V (to power the LM-158 AST op-amps), +5 V (to power the DS-2890's), one-wire, and

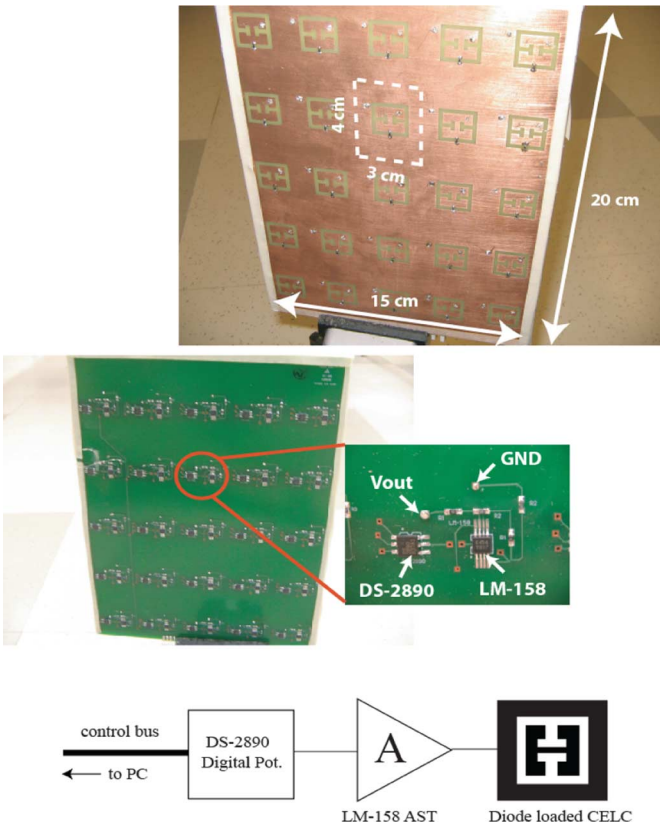

Fig. 2. (Top) Top view of the fabricated CELC metasurface reflectarray. The surface is 5×5 elements (15×20 cm^2), with each element 30 mm wide and 40 mm in height. (Middle) View of the bottom side of the metasurface reflectarray showing the control circuitry. (Bottom) The schematic shows how the LM-158 AST op-amp is used to amplify the output of the DS-2890.

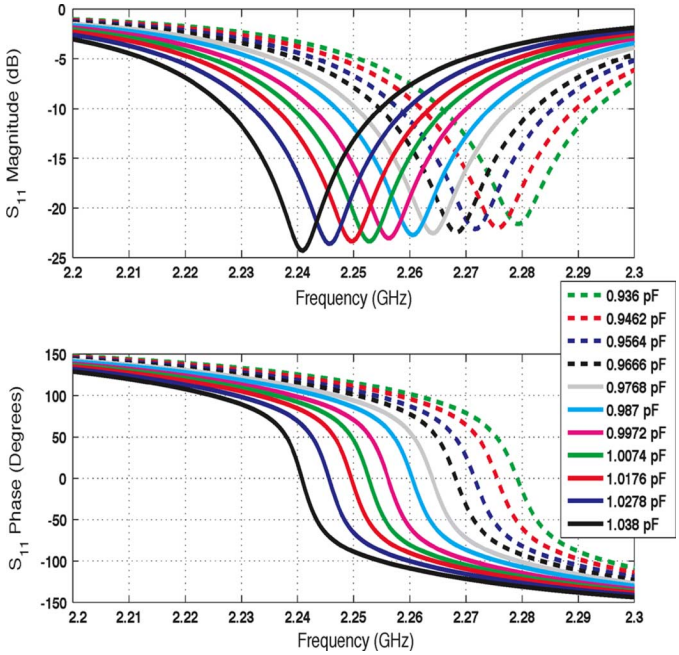

Fig. 3. Narrow sweep of $|\Gamma|$ and $\angle\Gamma$ for the varactor-loaded CELC particle from the HFSS simulation. When the varactor capacitance tunes from 0.63 to 2.67 pF, $\Delta\Gamma_{\rm p} \approx 340^\circ$ at 2.25 GHz (not shown).

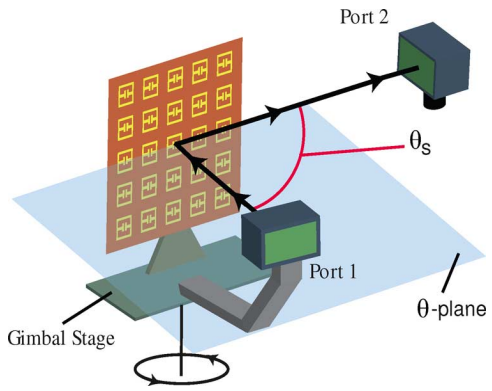

Fig. 4. Schematic illustrating how the reflection measurements were made. Two WR-340 waveguide adapters were used, where S_{21} is interpreted as the reflection off the surface. The picture shows measurements for $\theta_s = 90^\circ$, and the Gimbal stage rotates counterclockwise to cover scattered angles $-90^\circ \leq \theta_s \leq 90^\circ$. The shaded area denotes the θ-plane. Port 1 was placed approximately 30 cm from the surface, and port 2 was set back about 2 m from the surface.

ground. The +30 V and +5 V lines were connected to separate dc sources, and the one-wire line was connected to a PC serial port using a DS-9097U adapter, where software was used to located and control the state of the 25 digital potentiometers. The LM-158 AST operational amplifier was needed to provide an output voltage swing from 0–30 V since the DS-2890 can only output a maximum of +5 V. The noninverting amplifier configuration (with a gain of 6) was used to access the full range of varactor capacitances (0.63–2.67 pF). Although the unit cell width $d = 0.23\lambda_0$ is slightly large, this is necessary to keep the total reflectarray size greater than λ_0 while maintaining a reasonable number of elements. The unit cell size could be reduced, but this would increase the total number of unit cells in the reflectarray, forcing the need for a more complex automated biasing control network.

The addressable CELC surface was attached to a rotating Gimbal stage, where WR-340 adapters were used as the transmitting (port 1) and receiving (port 2) ports. Port 1 was placed at a fixed angle for normal incidence ($\theta_i = 0^\circ$) illumination of the CELC reflectarray. It was attached to the Gimbal stage and rotated with the reflectarray. Port 2 was fixed and positioned away from the Gimbal stage and elevated slightly to stay out of the shadow region of port 1. As the Gimbal stage rotated through 180°, port 2 received the reflected power with a resolution of 2°. With port 2 fixed and port 1 rotating with the surface so that θ_i is fixed at 0°, measuring the transmission from port 1 to port 2 (S_{21}) is effectively measuring the reflection off the CELC surface. A diagram showing how the fabricated addressable CELC reflectarray of Fig. 2 was measured is shown in Fig. 4. The Gimbal stage swept through 180° in 2° increments, measuring S_{21}, the scattered electric field energy, for $(-90^\circ \leq \theta_s \leq 90^\circ$ between 2–3 GHz.

The angle-resolved measurements were compared with an aluminum-plate control surface equal in physical size to the CELC surface. For the control measurement, it is expected that the peak reflected signal will occur in the specular direction ($\theta_s = \theta_i = 0^\circ$). With the width of the aluminum plate being slightly larger than the free-space wavelength λ_0, we expect the reflected signal to consist of a peak at $\theta_s = 0^\circ$ with a

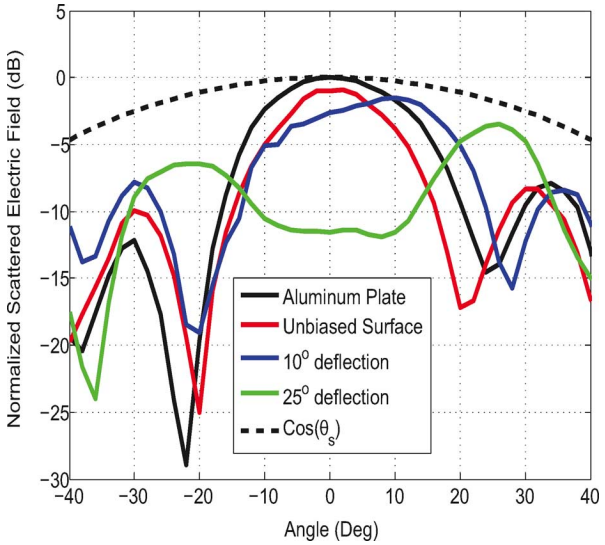

Fig. 5. Scattered electric field magnitude for 10° and 25° steering angles, with normal plane-wave incidence illumination. Each curve is normalized to the peak value of the metal plate. The sidelobes present are due to the finite size of the CELC reflectarray as well as the unequal amplitude weight on each particle.

TABLE I
SURFACE REQUIREMENTS FOR 10° DEFLECTION

10 Degree Deflection					
Req. Phase (deg)	124	138	152	166	181
Capacitance (pF)	0.936	0.868	1.038	0.63	2.67
Sim. Phase (deg)	125	137	152	162	-176
Sim. $\|\Gamma\|$, A_n	0.62	0.7	0.21	0.97	0.99
Reverse Bias V_{bias} (V)	10.01	12.39	7.44	30	0

TABLE II
SURFACE REQUIREMENTS FOR 25° DEFLECTION

25 Degree Deflection					
Req. Phase (deg)	-93	-121	-149	156	128
Capacitance (pF)	1.038	1.14	1.242	0.732	0.936
Sim. Phase (deg)	-60	-128	-150	157	126
Sim. $\|\Gamma\|$, A_n	0.1	0.66	0.858	0.944	0.622
Reverse Bias V_{bias} (V)	7.44	5.65	4.36	19.89	10.01

$\sin\theta_s/\theta_s$ profile. Fig. 5 shows the measurements of the addressable CELC surface with those of the aluminum plate. It is clear that the peak reflection does occur at the specular angle $\theta_s = \theta_i = 0°$ for the metal plate. All the measurements in Fig. 5 were plotted for a frequency $f = 2.3$ GHz. The single-element width $d = 3$ cm, and this information was used in (2) to get the necessary phase profile ψ_n to steer the peak $\theta' = 10°$ and 25°. The actual capacitances C_n needed for each ψ_n were found by modeling the CELC element of Fig. 1 in simulation using Ansoft HFSS. The required bias to realize each capacitance is given by $V(C) = (2.27/C)^{8/3} - 0.65$, which is the inversion of $C(V)$ discussed earlier. To steer the beam $-10°$ or $-25°$ away from the specular direction, the biases can simply be applied in the reverse order across the surface. Tables I and II show the requirements to steer a normally incident plane wave 10° and 25°. The required phase angle is the reflection coefficient phase angle necessary to deflect the incident plane wave $\varphi'°$ in accordance with (2). The capacitance to realize the phase close to the required phase (the simulated phase) is also shown, along with the simulated reflection coefficient magnitude $|\Gamma|$. The capacitance values were plugged into $V(C)$ to determine the necessary reverse bias across the varactor diodes. Notice how the peak scattered fields decrease in amplitude with increasing deflection angle, which is due to the decrease in effective area of the reconfigurable reflectarray relative to the receiving port for increasing angles of incidence. This scan loss is proportional to $\cos\theta_s$, which is also shown in Fig. 5.

The amplitude of the reflected wave for each CELC particle is different from unity due to losses in the copper, FR4 substrate, and varactor diode. Because we are operating near the resonant frequency of the CELC, $|\Gamma|$ changes significantly with bias. In reality, (1) is only an approximation to the true radiation pattern since it assumes a unit amplitude weight on each element. Simulations reveal that for the desired frequency of operation, the amplitude gradient across the surface is slightly smaller than 20 dB. From (1), it can be seen that a nonuniform spatial distribution in $|\Gamma|$ of this magnitude does not significantly affect the position of the radiation peak. It simply changes the level and shape of the sidelobes. Another cause of the nonnegligible sidelobe levels is error in the reflection coefficient phase angles.

V. SUMMARY

We developed a reconfigurable metamaterial reflectarray to scatter electromagnetic waves in a nonspecular direction. The surface consisted of addressable CELC metamaterials, and tuning the resonant frequency of each CELC to put a gradient in the reflection coefficient phase resulted in a scattered field profile that matched very closely with theoretical predictions. For two different potentiometer configurations, we were able to steer the peaks in the reflected energy 10° and 25° away from the specular direction. The large sidelobe levels were attributed to the nonuniform reflection coefficient amplitude across the surface as well as errors in the reflection coefficient phase angles.

REFERENCES

[1] J. B. Pendry, A. J. Holden, W. J. Stewart, and I. Youngs, "Extremely low frequency plasmons in metallic mesostructures," *Phys. Rev. Lett.*, vol. 76, no. 25, pp. 4773–4776, 1996.

[2] J. B. Pendry, A. J. Holden, D. J. Robbins, and W. J. Stewart, "Magnetism from conductors and enhanced nonlinear phenomena," *IEEE Trans. Microw. Theory Tech.*, vol. 47, no. 11, pp. 2075–2084, Nov. 1999.

[3] N. Engheta, "An idea for a thin subwavelength cavity resonator using metamaterials with negative permittivity and permeability," *IEEE Antennas Wireless Propag. Lett.*, vol. 1, pp. 10–13, 2002.

[4] S. A. Cummer, T. Hand, and N. Engheta, "The measured electric field spatial distribution within a metamaterial subwavelength cavity resonator," *IEEE Trans. Antennas Propag.*, vol. 55, no. 6, pp. 1781–1788, Jun. 2007.

[5] J. B. Pendry, "Negative refraction makes a perfect lens," *Phys. Rev. Lett.*, vol. 85, pp. 3966–3969, 2000.

[6] D. Schurig, J. J. Mock, and D. R. Smith, "Electric-field-coupled resonators for negative permittivity metamaterials," *Appl. Phys. Lett.*, vol. 88, no. 4, p. 041109, 2006.

[7] N. Riauka, A. Chauraya, and J. C. Vardaxoglou, "Compact antenna integrated into flat plate FSS," in *Proc. IEEE Antennas Propag. Soc. Int. Symp.*, Jul. 2008, pp. 1–4.

[8] G. Q. Luo, W. Hong, H. J. Tang, J. X. Chen, X. X. Yin, Z. Q. Kuai, and K. Wu, "Filtenna consisting of horn antenna and substrate integrated waveguide cavity FSS," *IEEE Trans. Antennas Propag.*, vol. 55, no. 1, pp. 92–98, Jan. 2007.

[9] C. H. Chan and R. Mittra, "Investigation of antenna interaction with an FSS radome," in *Proc. IEEE Antennas Propag. Soc. Int. Symp.*, Jun. 1989, vol. 2, pp. 1076–1079.
[10] S. J. Farmer, A. J. K. Laight, I. D. Grant, and K. C. Pitman, "Structural radar absorbent materials," in *Proc. IEE Colloq. Low Profile Absorbers Scatterers*, May 1992, pp. 2/1–2/4.
[11] A. J. Mackay, "The theory and design of provably optimal bandwidth radar absorbent materials (RAM) using dispersive structures and/or frequency selective surfaces (FSS)," in *Proc. ICEAA*, Sep. 2007, pp. 157–160.
[12] B. A. Munk*, Frequency Selective Surfaces*. New York: Wiley, 2000.
[13] C. L. Holloway, M. A. Mohamed, E. F. Kuester, and A. Dienstfrey, "Reflection and transmission properties of a metafilm: With an application to a controllable surface composed of resonant particles," *IEEE Trans. Electromagn. Compat.*, vol. 47, no. 4, pp. 853–865, Nov. 2005.
[14] E. F. Kuester, M. A. Mohamed, M. Piket-May, and C. L. Holloway, "Averaged transition conditions for electromagnetic fields at a metafilm," *IEEE Trans. Antennas Propag.*, vol. 51, no. 10, pp. 2641–2651, Oct. 2003.
[15] S. V. Hum, M. Okoniewski, and R. J. Davies, "Realizing an electronically tunable reflectarray using varactor diode-tuned elements," *IEEE Microw. Wireless Compon. Lett.*, vol. 15, no. 6, pp. 422–424, Jun. 2005.
[16] G. Angiulli, G. Amendola, G. Di Massa, F. Venneri, and L. Boccia, "Analysis and design of passive and active microstrip reflectarrays," *Int. J. RF Microw. Comput.-Aided Eng.*, vol. 13, no. 5, pp. 370–377, 2003.
[17] L. Mercier, E. Rodes, J. Drouet, L. Leger, E. Arnaud, M. Thevenot, T. Monediere, and B. Jecko, "Steerable and tunable EBG resonator antennas using smart metamaterials," in *Proc. IEEE Antennas Propag. Soc. Int. Symp.*, Jul. 2006, pp. 406–409.
[18] M. Caiazzo, S. Maci, and N. Engheta, "A metamaterial surface for compact cavity resonators," *IEEE Antennas Wireless Propag. Lett.*, vol. 3, pp. 261–264, 2004.
[19] L. Boccia, G. Amendola, and G. Di Massa, "Performance improvement for a varactor loaded reflectarray element," in *Proc. EuCAP*, Nov. 2007, pp. 1–3.
[20] H. Rajagopalan, Y. Rahmat-Samii, and W. A. Imbriale, "RF MEMS actuated reconfigurable reflectarray patch-slot element," *IEEE Trans. Antennas Propag.*, vol. 56, no. 12, pp. 3689–3699, Dec. 2008.
[21] T. H. Hand, J. Gollub, S. Sajuyigbe, D. R. Smith, and S. A. Cummer, "Characterization of complementary electric field coupled resonant surfaces," *Appl. Phys. Lett.*, vol. 93, no. 21, p. 212504, 2008.
[22] A. K. Bhattacharyya, "Radar cross section reduction of a flat plate by ram coating," *Microw. Opt. Technol. Lett.*, vol. 3, no. 9, pp. 324–327, 1990.
[23] W. J. R. Hoefer, S. A. Kosmopoulos, and A. Gagnon, "Nonlinear tlm modelling of high-frequency varactor multipliers and halvers," *Int. J. Infrared Millim. Waves*, vol. 3, no. 3, pp. 343–352, 1988.
[24] T. H. Hand and S. A. Cummer, "Controllable magnetic metamaterial using digitally addressable split-ring resonators," *IEEE Antennas Wireless Propag. Lett.*, vol. 8, pp. 262–265, 2009.